IV International Conference on Particle-based Methods – Fundamentals and Applications
PARTICLES 2015
E. Oñate, M. Bischoff, D.R.J. Owen, P. Wriggers & T. Zohdi (Eds)

ON SOME DRAWBACKS AND POSSIBLE IMPROVEMENTS OF A LAGRANGIAN FINITE ELEMENT APPROACH FOR SIMULATING INCOMPRESSIBLE FLOWS

MARCO LUCIO CERQUAGLIA[1], GEOFFREY DELIEGE[1], ROMAIN BOMAN[1], LUC PAPELEUX[1], VINCENT TERRAPON[1] AND JEAN-PHILIPPE PONTHOT[1]

[1] Department of Aerospace and Mechanical Engineering
University of Liège
Quartier Polytech 1, Allée de la Découverte 9, 4000 Liège (Belgium)
marcolucio.cerquaglia@ulg.ac.be; http://www.ltas.ulg.ac.be/

Key words: Particle finite element method, free surfaces, sloshing, dam break

Abstract. In this paper a Lagrangian finite element approach for the simulation of incompressible flows is presented, based on the so-called Particle Finite Element Method (PFEM). The spatial discretization and the definition of the boundary terms are discussed in detail with a specific focus on free-surface flows. Additionally, some problems that can arise from the use of such a method are pointed out. Some numerical examples are given and discussed in the last section of the paper.

1 INTRODUCTION

In the past decades numerical simulation of fluid flows has been mostly limited to Eulerian approaches, mainly due to the difficulty to treat extremely large deformations in a Lagrangian framework. On the other hand, the simulation of free-surface or multi-phase flows can become very difficult using an Eulerian description, due to the presence of interfaces, even if some techniques, such as the Volume Of Fluid (VOF) [4], have been developed in order to take the presence of interfaces into account.Up to a certain extent, these problems can be solved thanks to the Arbitrary Lagrangian-Eulerian (ALE) formulation [2]. Nevertheless, when it comes to problems involving complex free-surface flows, including mixing and separation, and possibly interacting with solid bodies, all the former approaches reach their limit, especially for industrial applications.
In this paper, we focus on the case of free-surface incompressible flows using a Lagrangian approach based on the Particle Finite Element Method (PFEM) [11]. In the first part of the paper a general description of the PFEM method is given. In the second part different

expressions of the governing equations are discussed, and spatial and time discretization are analyzed in more detail, together with some implementation issues. Finally, in the last part, some numerical examples are given.

2 THE PFEM METHOD

In the PFEM method the fluid is discretized using a set of points, referred to as *particles* hereafter, which actually represent material points of the body. In order to evaluate the forces acting on each particle, a new mesh is built at each time step, based on an Extended Delaunay Triangulation (EDT) [5], in such a way that the computational cost needed to evaluate nodal connectivity grows almost linearly with the number of particles [6]. At each remeshing the contours of the body are identified using the so-called α-*shape* technique [3]. Based on the new mesh, the Meshless Finite Element Method (MFEM) shape functions [7] can be defined in order to solve the corresponding weak form of the governing equations. The main steps of the PFEM method can be summarised as follows:

1. at a given time step, discretize the domain using a set of particles;
2. define the particle connectivity through an Extended Delaunay Triangulation (EDT);
3. identify the domain boundaries using the α-*shape* technique;
4. solve the governing equations using the MFEM shape functions;
5. use the solution obtained at the end of step 4 to update particles positions;
6. go back to step 2 and repeat the process for the next time step.

For a complete description of the method, refer e.g. to [11].
In the present implementation of the method, limited to 2D, a simple Delaunay triangulation is used, together with classical linear Finite Element shape functions, instead of MFEM ones.

3 GOVERNING EQUATIONS

The Navier-Stokes equations (momentum balance and mass conservation) for an incompressible Newtonian fluid in the current and reference configuration can be written, in Lagrangian form, as

$$\rho\frac{D\boldsymbol{u}}{Dt} = -\mathrm{grad}\,(p) + \mu\mathrm{div}\,(\mathrm{grad}\,(\boldsymbol{u})) + \mu\mathrm{div}\left(\mathrm{grad}\,(\boldsymbol{u})^T\right) + \rho\boldsymbol{b} \quad \text{in} \quad \Omega \tag{1}$$

$$\mathrm{div}\,(\boldsymbol{u}) = 0 \quad \text{in} \quad \Omega \tag{2}$$

and

$$\begin{aligned}\rho\frac{D\boldsymbol{U}}{Dt} = -\frac{1}{J}\mathrm{Div}\left(Jp\mathbf{F}^{-T}\right) + \frac{1}{J}\mu\mathrm{Div}\Big(J\mathrm{Grad}\,(\boldsymbol{U})\,\mathbf{F}^{-1}\mathbf{F}^{-T} + \\ J\mathbf{F}^{-T}\mathrm{Grad}\,(\boldsymbol{U})^T\,\mathbf{F}^{-T}\Big) + \rho\boldsymbol{b} \quad \text{in} \quad \Omega_0\end{aligned} \tag{3}$$

$$\mathrm{Div}\left(J\mathbf{F}^{-1}\boldsymbol{U}\right) = 0 \quad \text{in} \quad \Omega_0 \tag{4}$$

respectively, where Ω and Ω_0 are the volumes occupied by the fluid in the current and reference configuration, $\rho(\boldsymbol{x},t)$ is the density, $\mu(\boldsymbol{x},t)$ is the viscosity, $\boldsymbol{u} = \boldsymbol{u}(\boldsymbol{x},t)$ is the velocity vector, $p(\boldsymbol{x},t)$ is the pressure, and $\rho\boldsymbol{b}(\boldsymbol{x},t)$ is a body force, such as gravity for instance. $D(\cdot)/Dt$ is the Lagrangian, or material, derivative of the quantity $(\cdot)$, $\mathbf{F} = \frac{d\boldsymbol{x}}{d\boldsymbol{X}}$ is the deformation gradient and $J = \det(\mathbf{F})$. Capital letters are used to denote quantities defined in the reference configuration.
These equations have to be complemented with Dirichlet and Neumann boundary conditions:

$$\boldsymbol{u}(\boldsymbol{x},t) = \bar{\boldsymbol{u}}(\boldsymbol{x},t) \quad \forall \boldsymbol{x} \in \Gamma_D \tag{5}$$

$$\boldsymbol{\sigma}(\boldsymbol{x},t)\cdot\boldsymbol{n} = \bar{\boldsymbol{t}}(\boldsymbol{x},t) \quad \forall \boldsymbol{x} \in \Gamma_N, \tag{6}$$

where $\bar{\boldsymbol{u}}(\boldsymbol{x},t)$ and $\bar{\boldsymbol{t}}(\boldsymbol{x},t)$ are imposed velocities and surface tractions respectively, $\boldsymbol{\sigma} = \boldsymbol{\sigma}(\boldsymbol{x},t)$ is the Cauchy stress tensor, $\boldsymbol{n}$ denotes the unit outward normal to the boundary, $\Gamma_D \cup \Gamma_N = \partial\Omega$ and $\Gamma_D \cap \Gamma_N = \emptyset$.

3.1 Weak form and spatial discretization

For further developments, only the forms corresponding to Equations (3) and (4) will be discussed, the developments related to the current configuration being the same.
Introducing the following spaces for trial and test functions

$$\begin{aligned} S &= \left\{\boldsymbol{U} \in \mathbf{H}^1(\Omega) \,|\boldsymbol{U} = \bar{\boldsymbol{U}} \quad \text{on} \quad \Gamma_D\right\}, \\ S_0 &= \left\{\boldsymbol{W} \in \mathbf{H}^1(\Omega) \,|\boldsymbol{W} = \boldsymbol{0} \quad \text{on} \quad \Gamma_D\right\}, \\ Q &= \left\{q \in L^2(\Omega)\right\}, \end{aligned}$$

the weak form of Equations (3) and (4) can be established by multipling Equation (3) by a vector test function $\boldsymbol{W} \in S_0$ and Equation (4) by a scalar test function $q \in Q$. Integrating over the reference volume and using Green theorem, the weak form finally reads

$$\begin{aligned} \int_{\Omega_0} \rho_0 \frac{D\boldsymbol{U}}{Dt}\cdot\boldsymbol{W}\mathrm{d}\Omega_0 &= \int_{\Omega_0} Jp\mathbf{F}^{-T} : \mathrm{Grad}(\boldsymbol{W})\,\mathrm{d}\Omega_0 \\ -\int_{\Omega_0} \mu J\left[\mathrm{Grad}(\boldsymbol{U})\,\mathbf{F}^{-1}\mathbf{F}^{-T} : \mathrm{Grad}(\boldsymbol{W}) + \mathbf{F}^{-T}\mathrm{Grad}(\boldsymbol{U})^T\,\mathbf{F}^{-T} : \mathrm{Grad}(\boldsymbol{W})\right]\mathrm{d}\Omega_0 \\ + \int_{\Omega_0} \rho_0\boldsymbol{b}\cdot\boldsymbol{W}\mathrm{d}\Omega_0 + \int_{\Gamma_N} \boldsymbol{W}\cdot\bar{\boldsymbol{t}}\mathrm{d}\Gamma_N \quad \forall \boldsymbol{W} \in S_0, \end{aligned} \tag{7}$$

$$\int_{\Omega_0} \mathrm{Div}\left(J\mathbf{F}^{-1}\boldsymbol{U}\right) q\,\mathrm{d}\Omega_0 = 0 \quad \forall q \in Q. \tag{8}$$

Equations (7) and (8) can be discretized using linear isoparametric finite elements, leading to the following system of semi-discrete equations:

$$\mathbf{M}\frac{D\boldsymbol{V}}{Dt} + \mathbf{K}\boldsymbol{V} + \mathbf{D}^T\boldsymbol{P} = \boldsymbol{B}, \tag{9}$$

$$\mathbf{D}\boldsymbol{V} = \mathbf{0}, \tag{10}$$

where $\mathbf{M}$ is the mass matrix (that can be lumped if needed), $\mathbf{K}$ the matrix containing the viscous terms, $\mathbf{D}$ the discrete version of the divergence operator, and $\boldsymbol{B}$ a vector containing the contribution of body forces and surface tractions. Spatial integration can be performed using classical Gauss integration (1 Gauss point per linear triangle in 2D).

3.2 Pressure stabilization and boundary terms

Pressure stabilization The selected discretization, i.e. linear velocity and pressure, is known to violate the Ladyzhenskaya-Babuška-Brezzi (LBB) condition. To circumvent this problem a Petrov-Galerkin pressure stabilization procedure has been preferred over a fractional step method as it shows better mass conservation properties, as discussed in [1].
The approach used here is the one adopted by Tezduyar *et al.* [13] and consists in adding to the mass conservation equation an integral term defined as the product of a stabilizing parameter τ^e_{PSPG} (see [13]) and the residual of the momentum equation.
The stabilized version of Equation (8) is then

$$\begin{aligned}\int_{\Omega_0} \mathrm{Div}\left(J\mathbf{F}^{-1}\boldsymbol{U}\right) q \mathrm{d}\Omega_0 + \sum_{e=1}^{N_{el}} \int_{\Omega_0} \tau^e_{\mathrm{PSPG}} \frac{1}{\rho_0}\mathrm{Grad}\left(q\right)\Bigg(\rho_0\frac{D\boldsymbol{U}}{Dt} + \frac{1}{J}\mathrm{Div}\left(Jp\mathbf{F}^{-T}\right) - \\ \frac{1}{J}\mu\mathrm{Div}\left(J\mathrm{Grad}\left(\boldsymbol{U}\right)\mathbf{F}^{-1}\mathbf{F}^{-T} + J\mathbf{F}^{-T}\mathrm{Grad}\left(\boldsymbol{U}\right)^T\mathbf{F}^{-T}\right) - \rho_0\boldsymbol{b}\Bigg) = 0 \quad \forall q \in Q.\end{aligned} \tag{11}$$

By neglecting the higher-order term $\mathrm{Div}\left(J\mathrm{Grad}\left(\boldsymbol{U}\right)\mathbf{F}^{-1}\mathbf{F}^{-T} + J\mathbf{F}^{-T}\mathrm{Grad}\left(\boldsymbol{U}\right)^T\mathbf{F}^{-T}\right)$, the equations to be solved can be finally summarized as follows

$$\mathbf{M}\frac{D\boldsymbol{V}}{Dt} + \mathbf{K}\boldsymbol{V} + \mathbf{D}^T\boldsymbol{P} = \boldsymbol{B}, \tag{12}$$

$$\mathbf{C}\frac{D\boldsymbol{V}}{Dt} + \mathbf{D}\boldsymbol{V} + \mathbf{L}\boldsymbol{P} = \boldsymbol{H}. \tag{13}$$

Boundary terms A further important remark has to be made regarding the form of the equations proposed in the present work and in particular the treatement of boundary terms.
When dealing with incompressible Newtonian fluids the Navier-Stokes equations are often written in so-called *Laplace form*, since the term $\mu\mathrm{div}\left(\mathrm{grad}\left(\boldsymbol{u}\right)\right) + \mu\mathrm{div}\left(\mathrm{grad}\left(\boldsymbol{u}\right)^T\right)$ in

Equation (1) simplifies to $\mu \text{div}\left(\text{grad}\left(\boldsymbol{u}\right)\right) = \mu \Delta \boldsymbol{u}$. Even if this is correct from a physical point of view, it has some consequences for the expression of the weak form of the equations.
In particular, the correct natural boundary condition for the Laplace weak form of the Navier-Stokes equations is

$$\int_{\Gamma_N} \boldsymbol{W} \cdot \bar{\boldsymbol{t}} \mathrm{d}\Gamma_N - \int_{\Gamma_N} \boldsymbol{W} \cdot \left[\mu \text{grad}\left(\boldsymbol{u}\right)^T\right] \cdot \boldsymbol{n} \mathrm{d}\Gamma_N. \tag{14}$$

Therefore, the 'physical' boundary condition $\int_{\Gamma_N} \boldsymbol{W} \cdot \bar{\boldsymbol{t}} \mathrm{d}\Gamma_N$, containing the surface tractions, is *not* the natural boundary condition that derives from the Navier-Stokes equations written in Laplace form.
Some authors do not account for this subtlety, even if it leads to a violation of the objectivity principle, as discussed in [10], and neglect the second term appearing in Equation (14).
In this work the Navier-Stokes equations are written in *divergence form* so that the boundary term $\int_{\Gamma_N} \boldsymbol{W} \cdot \bar{\boldsymbol{t}} \mathrm{d}\Gamma_N$ represents simultaneously both a 'physical' and a natural boundary condition.

3.3 Time integration

Time integration is performed using an implicit backward-Euler scheme.
Positions at time t^{n+1} are computed as

$$\boldsymbol{X}^{n+1} = \boldsymbol{X}^n + \boldsymbol{V}^{n+1} \Delta t, \tag{15}$$

which leads to the system of fully-discrete equations

$$\begin{bmatrix} \frac{1}{\Delta t}\mathbf{M}^{n+1} + \mathbf{K}^{n+1} & \mathbf{D}^{Tn+1} \\ \frac{1}{\Delta t}\mathbf{C}^{n+1} + \mathbf{D}^{n+1} & \mathbf{L}^{n+1} \end{bmatrix} \begin{Bmatrix} \boldsymbol{V}^{n+1} \\ \boldsymbol{P}^{n+1} \end{Bmatrix} = \begin{Bmatrix} \boldsymbol{B}^{n+1} + \frac{1}{\Delta t}\mathbf{M}^{n+1}\boldsymbol{V}^n \\ \boldsymbol{H}^{n+1} + \frac{1}{\Delta t}\mathbf{C}^{n+1}\boldsymbol{V}^n \end{Bmatrix}. \tag{16}$$

Due to the implicit time integration, Equations (16) are non-linear so that an iterative algorithm has to be used to find the solution at time t^{n+1}. As discussed in [8] a Picard algorithm is preferable to a Newton-Raphson algorithm in this case.

3.4 Problems related to remeshing

In the present approach a problem can arise due to the continuous remeshing of the domain. In particular, since for quantities that are not defined at the nodes, such as stresses, no proper projection is made from the old mesh to the new one, perturbations of the solution can appear after a remeshing. In other words, the solution is no longer C^0 continuous in time.
To the best of our knowledge, this is the first time in the literature that this problem related to the PFEM method is addressed. We will first try to give some justification of what happens and then suggest some ideas on how to alleviate the problem.

Problem description Let us suppose that the equilibrium at time n has been reached: nodes are moved to the new position $\boldsymbol{X}^{n+1}$ and a remeshing takes place, leading to an unequilibrated configuration.
There are two contributions to this new out-of-balance configuration: the first one comes from the fact that the physical problem is not at equilibrium anymore and the second one from the fact that the equilibrium at time n was computed on a different mesh and there is no guarantee that the same equilibrium solution would have exactly held on the new mesh. The latter can introduce some perturbations in the velocity and pressure fields: we will denote these perturbations on velocity and pressure as $\delta\boldsymbol{V}^{n+1}$ and $\delta\boldsymbol{P}^{n+1}$, respectively.
The momentum equation that has to be verified at time $n+1$ becomes

$$\mathbf{M}\left(\frac{\bar{\boldsymbol{V}}^{n+1}+\delta\boldsymbol{V}^{n+1}-\boldsymbol{V}^{n}}{\Delta t}\right)+\mathbf{K}\left(\bar{\boldsymbol{V}}^{n+1}+\delta\boldsymbol{V}^{n+1}\right)+\mathbf{D}^{T}\left(\bar{\boldsymbol{P}}^{n+1}+\delta\boldsymbol{P}^{n+1}\right)=\boldsymbol{B}, \quad (17)$$

where $\bar{}$ quantities are solution to the physical (unperturbed) equilibrium. If physical equilibrium is satisfied, then Equation (17) becomes

$$\underbrace{\mathbf{M}\frac{\delta\boldsymbol{V}^{n+1}}{\Delta t}}_{\text{(a)}}+\underbrace{\mathbf{K}\delta\boldsymbol{V}^{n+1}}_{\text{(b)}}+\underbrace{\mathbf{D}^{T}\delta\boldsymbol{P}^{n+1}}_{\text{(c)}}=\mathbf{0}. \quad (18)$$

Term (b) is directly defined by the velocity field perturbation $\delta\boldsymbol{V}^{n+1}$ and for dynamic problems, if this perturbation is finite but small, this term is small with respect to the other two. On the contrary, term (a) is amplified by the presence of the time step Δt. If one wants Equation (18) to be satisfied, the only contribution that can counter-balance the first term comes from term (c), which therefore results in oscillations of the pressure field. Evidence of this phenomenon is given in section 4.

Possible remedies The amplitude of pressure oscillations is proportional to the extra inertial force (a). Term (a) is proportional to the velocity jump $\delta\boldsymbol{V}^{n+1}$ (which itself depends on the problem and on the mesh size) and inversely proportional to time step Δt. Thus, in general, pressure oscillations decrease for finer meshes and larger time steps.

4 NUMERICAL EXAMPLES

In this section some numerical applications of the present approach are presented.

4.1 Sloshing problem

In this example the free sloshing of an incompressible Newtonian fluid in a rigid reservoir is considered, as depicted in Figure 1. This problem has already been studied in

the literature (see for instance [1, 12]), so it represents a good benchmark to validate our code.

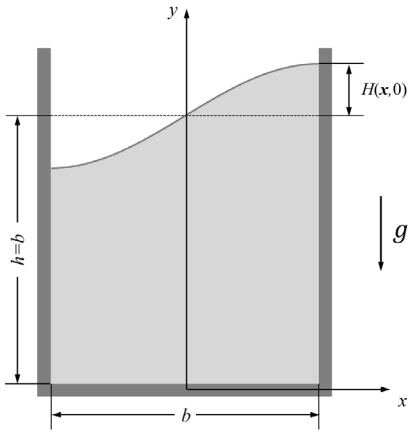

Figure 1: Sloshing problem. A fluid is placed in a reservoir and an initial out-of-balance configuration is enforced through the free-surface profile definition.

The initial free-surface profile is defined as

$$H\left(\boldsymbol{x},0\right)=a\sin\left(\pi\frac{x}{b}\right), \tag{19}$$

where b is the width of the reservoir, H denotes the free-surface height with respect to the average level and a is the initial amplitude. In this case values of $a = 0.01$ m and $b = 1.0$ m, as well as fictitious values of fluid viscosity $\mu = 0.01$ kg/ms, density $\rho = 1.0$ kg/m^3 and gravity $g = 1.0$ m/s^2 are considered. For the calculation, an initial discretization of 1166 nodes and 2330 triangles and a constant time step of 0.01 s are used. A free-slip condition is enforced on the container walls.
Figure 2 presents the time evolution of the free surface at $x = \pm b/2$. Circles denote values obtained from [12] and triangles from [1]. Very good agreement is observed, especially with the solution provided by Radovitzky and Ortiz [12]. For this problem a maximum relative error of $5 \cdot 10^{-4}\%$ on mass conservation is obtained.

Remeshing issues A numerical example is proposed to illustrate the problems described in section 3.4, related to continuous remeshing.
The example is again a sloshing problem, as presented above, but this time a very coarse mesh is employed, in order to better highlight the issue. Moreover values of $\rho = 1000$ kg/m^3 and $g = 9.81$ m/s^2 are used. The initial mesh is depicted in Figure 3. During the simulation, if remeshing is performed at each time step, four possible configurations exist, as depicted in Figure 4. Results are shown in Figures 5 and 6. All the analyses are performed with a time step of 0.001 s.

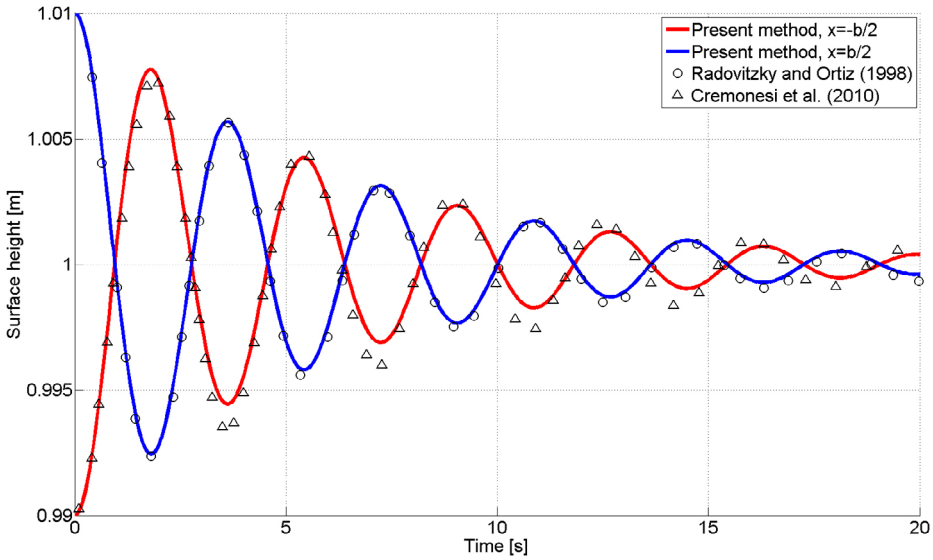

Figure 2: Sloshing problem. Time evolution of the position of the free-surface at $x = -b/2$ and $x = b/2$: very good agreement with other authors' results is found, especially the one obtained by Radovitzky and Ortiz [12].

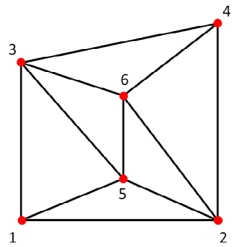

Figure 3: Remeshing issues: initial mesh. An extremely coarse mesh (with only 6 nodes) is used in order to better understand the influence of remeshing on the results.

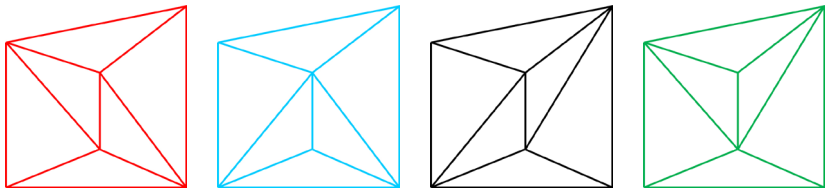

(a) Mesh 1 (b) Mesh 2 (c) Mesh 3 (d) Mesh 4

Figure 4: Remeshing issues. Four different configurations can be obtained during the simulation due to remeshing: they correspond to meshes 1, 2, 3 and 4.

In Figure 5 the velocity along the y-direction of node 5 for the case with continuous remeshing is displayed and compared to results obtained for meshes 1-4 without remeshing. Colored images are used to symbolize the configuration of the remeshing case that corresponds to a given portion of the simulation.

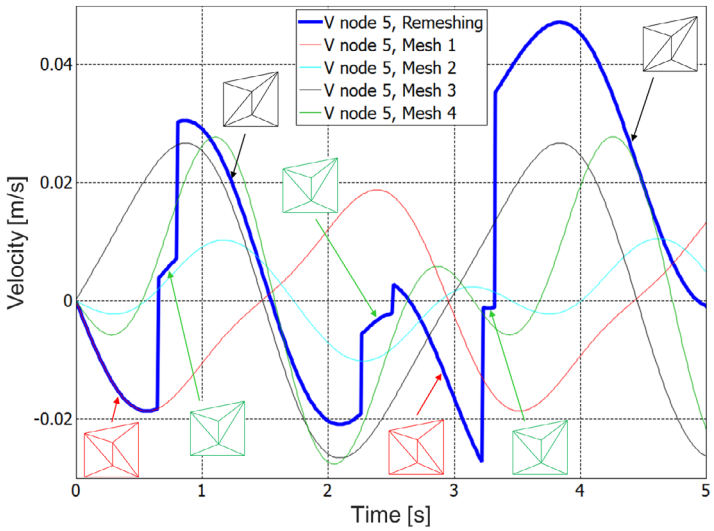

Figure 5: Remeshing issues: node 5 velocity along the y-direction. The thick blue line represents the case where a remeshing is performed at each time step, while thin lines are the results obtained for meshes 1-4 (see Figure 4) without remeshing. Colored images indicate the configuration of the continuous remeshing case that corresponds to a given part of the simulation. Whenever the configuration changes, discontinuities appear in the velocity field due to the fact that the discrete solution can be different from one mesh to another.

First of all, as it could be expected for such a coarse mesh, four different results are obtained for the four meshes. Moreover, for the continuous remeshing case, it can be seen that remeshing can introduce discontinuities in the velocity field. This can be expected in view of the very different solutions the four configurations without remeshing can lead to. To better understand the implications of this observation on the results, Figure 6(a) shows the evolution of inertial, internal and external forces along the y-direction at node 5. Inertial forces represent the term $\mathbf{M}\frac{D\boldsymbol{V}}{Dt}$ in Equation (12), internal forces the term $\mathbf{K}\boldsymbol{V} + \mathbf{D}^T\boldsymbol{P}$ and external forces the term $\boldsymbol{B}$.
As discussed in section 3.4 jumps of inertial forces can be observed after remeshing (corresponding to the larger velocity jumps), to which correspond discontinuities in the internal forces, which, in this case, basically corresponds to the pressure gradient.
In Figure 6(b) one can observe the strong discontinuities appearing in the pressure field, due to the perturbations introduced by the remeshing. As previously discussed, it can be observed that for a larger time step, i.e. 0.01 s, the pressure peaks are strongly attenuated.

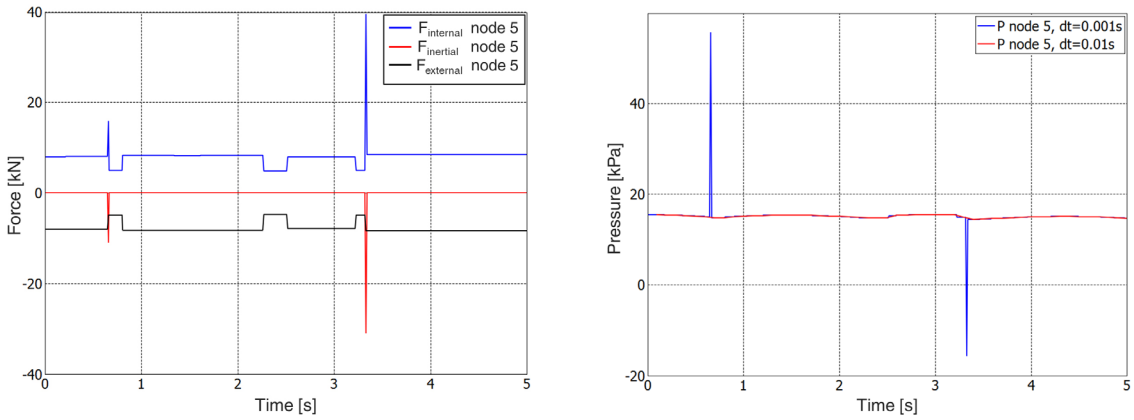

(a) Forces along the y-direction at node 5

(b) Pressure at node 5

Figure 6: Remeshing issues. Perturbations induced by the remeshing in the velocity field cause strong discontinuities in the inertial term, that have to be counter-balanced by internal forces (a), in particular by the pressure gradient. Strong oscillations in the pressure field (b) correspond to discontinuities in the velocity field induced by remeshing (peaks in the blue curve). A larger time step reduces them, since smaller accelerations are induced by velocity perturbations.

Again, this phenomenon will also become less and less visible for finer and finer meshes.

4.2 Dam break

The dam break problem is a classical benchmark for the analysis of free-surface flows. The problem is depicted in Figure 7 and consists in a column of water in a container, initially held by a rigid wall. The wall is instantaneously removed and the motion of the water is studied.
In this case a length $L = 0.146$ m is considered. Classical values for water properties are chosen, that is a density $\rho = 1000$ kg/m^3 and a dynamic viscosity $\mu = 0.001$ kg/ms. An initial mesh of 1650 nodes and 3171 elements, and a time step of 0.02 s are used. A no-slip condition is enforced on container walls. The solutions obtained at different time steps are shown in Figure 8 and compared to experimental results obtained by Koshizuka and Oka [9]. Again, a good agreement is observed.

5 CONCLUSIONS

A Lagrangian finite element approach for the study of incompressible flows, based on the PFEM method, has been presented.
Particular attention has been devoted to the mathematical formulation of the method and to the correct definition of the weak form, in particular concerning boundary terms. The validity and robustness of the approach have been assessed on some simple examples.

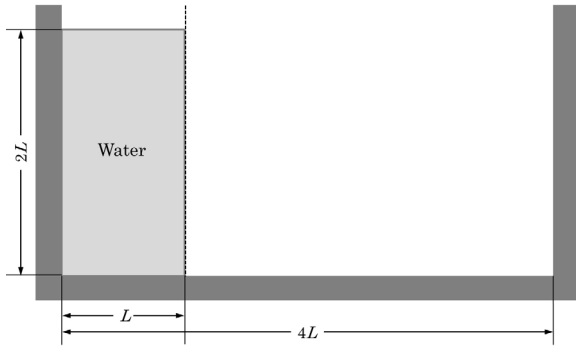

Figure 7: Dam break problem. The water column is initially held by a rigid wall. The wall is suddenly removed and the motion of the fluid is regarded.

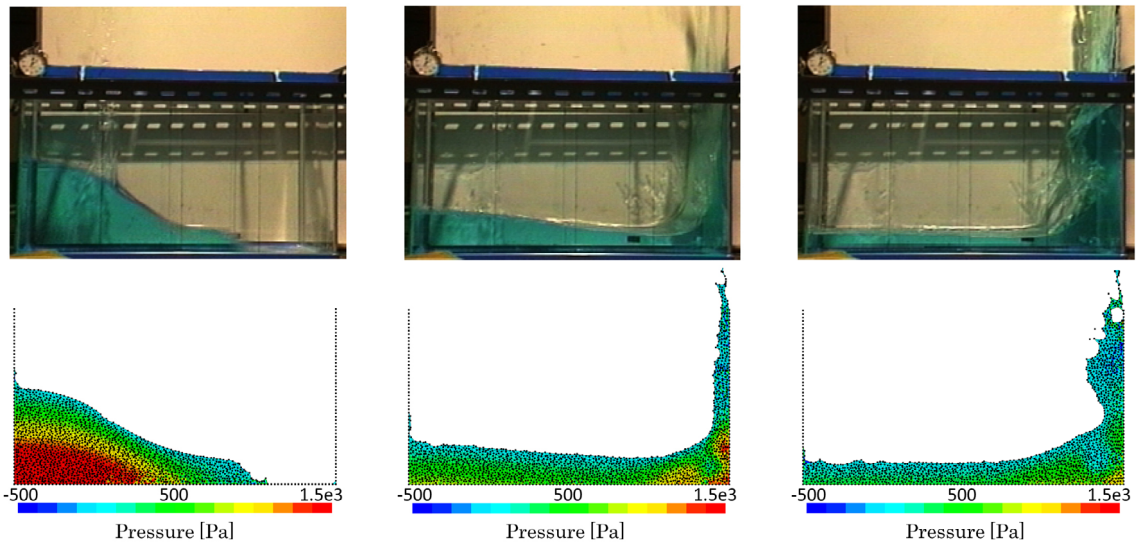

(a) $t = 0.2$s (b) $t = 0.4$s (c) $t = 0.6$s

Figure 8: Dam break problem. Comparison between experimental results taken from [9] (top) and numerical ones (bottom). The evolution of the water column is displayed at times $t = 0.2$ s (a), $t = 0.4$ s (b) and $t = 0.6$ s (c): good agreement with experimental results can be seen. Pressure field is also shown for the numerical solution.

Finally, some problems related to the continuous remeshing procedure used in the present method have been pointed out. It was shown that some perturbations are introduced by the remeshing in the velocity field: these perturbations can be amplified by a small time step, leading to large accelerations that have to be compensated by the pressure gradient, resulting in large oscillations in the pressure field, if the mesh is not fine enough. No

solution to this problem has been found so far, but it is a perspective for future works.

REFERENCES

[1] Cremonesi M., Frangi A. and Perego U. A Lagrangian finite element approach for the analysis of fluid-structure interaction problems. *Int. J. Num. Meth. Engng.* (2010) **84**:610–630.

[2] Donea J., Huerta A., Ponthot J.P. and Rodríguez-Ferran A. *Encyclopedia of Computational Mechanics, Stein E., de Borst R., Hughes T.J.R. (eds)*. John Wiley & Sons (2004).

[3] Edelsbrunner H. and Mucke E.P. Three dimensional alpha shapes. *ACM Transaction on Graphics* (1994) **13**(1):43–72.

[4] Hirt C.W., Nichols B.D. Volume of fluid (VOF) method for the dynamics of free boundaries. *J. Comput. Physics* (1981) **39**:201–225.

[5] Idelsohn S., Calvo N. and Oñate E. Polyhedrization of an arbitrary 3D point set. *Comput. Methods Appl. Mech. Engrg.* (2003) **192**:2649–2667.

[6] Idelsohn S. and Oñate E. To mesh or not to mesh. That is the question... *Comput. Methods Appl. Mech. Engrg.* (2006) **195**:4681–4696.

[7] Idelsohn S., Oñate E., Calvo N. and Del Pin F. The meshless finite element method.*Int. J. Num. Meth. Engng.* (2003) **58**:893–912.

[8] Idelsohn S., Oñate E., Del Pin F., Calvo N. Fluid–structure interaction using the particle finite element method. *Comput. Methods Appl. Mech. Engrg.* (2006) **195**:2100–2123.

[9] Koshizuka S. and Oka Y. Moving particle semi-implicit method for fragmentation and incompressible fluid. *Nuclear science and engineering* (1996) **123**:421–434.

[10] Limache A. and Idelsohn S. Laplace form of Navier-Stokes equations: a safe path or a wrong way? *Mecánica Computacional* (2006) **25**:151–168.

[11] Oñate E., Idelsohn S., Del Pin F. and Aubry R. The particle finite element method. An overview. *Int. J. Comput. Methods* (2004) **61**:964–989.

[12] Radovitzky R. and Ortiz M. Lagrangian finite element analysis of Newtonian fluid flows. *Int. J. Num. Meth. Engng.* (1998) **43**:607–619.

[13] Tezduyar T.E., Mittal S., Ray S.E., Shih R. Incompressible flow computations with stabilized bilinear and linear equal-order-interpolation velocity-pressure elements. *Comput. Methods Appl. Mech. Engrg.* (1992) **95**(2):221–242.